(1+1)-dimensional turbulence

R. Benzi[a)]
AIPA, Via Po 14, 00100 Roma, Italy

L. Biferale
INFM-Dipartimento di Fisica, Università di Tor Vergata, Via della Ricerca Scientifica 1, I-00133 Roma, Italy

R. Tripiccione
INFN, Sezione di Pisa, S. Piero a Grado, I-50100 Pisa, Italy

E. Trovatore
INFM-Dipartimento di Fisica, Università di Cagliari, Via Ospedale 72, I-09124, Cagliari, Italy

(Received 2 October 1996; accepted 4 March 1997)

A class of dynamical models of turbulence living on a one-dimensional dyadic-tree structure is introduced and studied. The models are obtained as a natural generalization of the popular GOY shell model of turbulence. These models are found to be chaotic and intermittent. They represent the first example of (1+1)-dimensional dynamical systems possessing non trivial multifractal properties. The dyadic structure allows us to study spatial and temporal fluctuations. Energy dissipation statistics and its scaling properties are studied. The refined Kolmogorov hypothesis is found to hold. © *1997 American Institute of Physics.* [S1070-6631(97)00708-3]

I. INTRODUCTION

Spatio-temporal intermittency is the most intriguing aspect of a fully developed three-dimensional turbulent flow. Turbulent structures are thought to be generated by chaotic intermittent energy transfer from large to small scales. The cascade is pictorially described by the Richardson scenario: large scale eddies destabilize and generate small scale eddies with shorter eddy turnover times. In this way, a hierarchy of fluctuations on smaller and smaller scales and with shorter and shorter characteristic times is produced.

Kolmogorov 1941 theory[1] describes the statistics of velocity differences, $\delta_r v$, at scale r in terms of the averaged energy dissipation ε, neglecting completely possible spatio-temporal fluctuations. The velocity field statistics is characterized, among others, by the scaling exponents, $\zeta(p)$, of structure functions $S_p(r)$, in the inertial range:

$$S_p(r) \equiv \langle |v(x+r)-v(x)|^p \rangle \equiv \langle |\delta_r v|^p \rangle \sim r^{\zeta(p)}. \tag{1}$$

In the Kolmogorov description, a simple dimensional argument leads to the predictions

$$\langle |\delta_r v|^p \rangle \sim \varepsilon^{p/3} r^{p/3}; \quad \zeta(p) = p/3.$$

On the other hand, experiments show[2] that scaling exponents deviate from the linear behavior. This departure from linearity is the main signature of intermittency and implies non-Gaussian probability distribution functions for the velocity differences in the inertial range.

Intermittency also affects energy dissipation statistics. Experiments[3] show that the energy dissipation defines a multifractal measure on the fluid volume. The multifractal measure is characterized by the scaling properties of the coarse-grained energy dissipation, ε_r, namely,

$$\langle \varepsilon_r^p \rangle \equiv \left\langle \left(\frac{1}{r^3} \int_{\Lambda(r)} d^3x \varepsilon(x) \right)^p \right\rangle \sim r^{\tau(p)}, \tag{2}$$

where $\langle \cdot \rangle$ means averaging over all boxes $\Lambda(r)$ of size r in which the volume occupied by the fluid is partitioned.

The celebrated refined Kolmogorov hypothesis (RKH)[4] links the statistics of velocity differences in the inertial range with the statistics of the coarse-grained energy dissipation:

$$\frac{(\delta_r v)^3}{r} \sim \varepsilon_r, \tag{3}$$

where the symbol $\sim$ means that quantities on both sides have the same scaling properties.

Using (3), it is easy to relate the scaling exponents $\zeta(p)$ with the scaling exponents of the energy dissipation:

$$\zeta(p) = \tau(p/3) + p/3. \tag{4}$$

This relation is the natural consequence of the RKH and it is quite well satisfied experimentally.[5] On the other hand, no satisfactory theoretical arguments which predict (4) have ever been found.

The simplest way to explain phenomenologically the presence of intermittent deviations consists in describing the energy transfer mechanism in terms of fragmentation stochastic processes. In these models,[3,6,7] one introduces a set of eddies leaving on a dyadic structure.

Random fragmentation models state that the energies contained in eddies at successive scales are connected to each other by independent stochastic variables with a distribution that does not depend on the scale. For example, in the random-β-model we have $\varepsilon_n = \beta \varepsilon_{n+1}$, where ε_n denotes the energy transfer due to a typical eddy of size $r_n = 2^{-n} r_0$. In the random-β-model also the active volume, V_n, occupied by eddies of size r_n, is supposed to change randomly from scale to scale: $V_{n+1} = \beta V_n$. From the definition (2) we have $\tau(p) = -\log_2 \langle \beta^{p-1} \rangle$ and the corresponding expression $\zeta(p) = p/3 - \log_2 \langle \beta^{p/3-1} \rangle$ must be valid if the RKH holds.

[a)]On leave on absence from the Dipartimento di Fisica, Università di Tor Vergata.

Due to the freedom in the choice of the β distribution all these models are able to fit with good accuracy experimental values. On the other hand, they lack any direct linking with the original Navier–Stokes (NS) equations.

In this paper, we investigate a class of dynamical models which fill the gap between purely stochastic fragmentation models and the original NS dynamics. In particular, we define and study a dynamical model on a (1+1)-dimensional (that is, having space and time dimensions) dyadic tree. We decompose the original velocity field in terms of fluctuations localized both in Fourier and real spaces. One can look at this model as an approximation of the original NS equations in a wavelet basis (see the next section).

Previous (1+1)-dimensional models studied in the past[8,9] did not seem to develop nontrivial dynamics. More recently, (1+3)-dimensional dynamical tree models have been investigated by Grossmann and coworkers,[10,11] in the same spirit of our work. These models have been obtained directly from NS equations, using a spatially resolved Fourier–Weierstrass decomposition, and have been shown to possess multifractal properties.

At a difference from the models studied in Refs. 10 and 11, we do not impose all the original geometrical constraints of the NS equations. For example, we do not have neither divergenceless velocity fields nor three-dimensional structures of the real space. In this way we can embed the model in a one-dimensional real space and simplify enormously the structure of the nonlinear terms.

The most important advantage is that we can increase the total number of resolved scales (and therefore we can reach high Reynolds numbers), paying the price of having a model which is not exactly derivable from the original NS equations.

The main result of this paper is to present for the first time a one-dimensional dynamical system sharing some of the most important properties with a real three-dimensional turbulent flow. In particular, we analyze structure function intermittency and the energy dissipation spatial distribution. RKH is found to be remarkably well satisfied. These models are the natural ground where testing new developments of large-dimensional dynamical-system theory and new approaches to turbulent (i.e., multi-scale systems) flows. As we discuss in the following, numerical simulations need state-of-the-art multi-processor computers.

The paper is organized as follows. In Sec. II, we discuss how to jump from zero-dimensional shell models to one-dimensional spatially resolved tree models; the tree model is introduced in Sec. III; in Sec. IV, numerical results on structure functions intermittency, viscous scales dynamics and energy dissipation field statistics are presented; conclusions follow in Sec. V.

II. FROM CHAINS TO TREES

In order to understand turbulent energy transfer dynamics and related intermittent effects, dynamical deterministic models have been proposed. Among these models, shell models have recently attracted the interests of many researchers (see Ref. 12 for a popular introduction). The basic idea in such models is to retain only a few variables as representative of an entire *shell* of Fourier amplitudes. The non linear structure of NS equations is preserved, but all three-dimensional properties of the original embedding space are lost.

The most popular shell model is the Gledzer–Ohkitani–Yamada (GOY) model (Refs. 13–18). The GOY model can be seen as a severe truncation of the NS equations. Dynamical variables are described by a single complex mode u_n for each shell of wave numbers k such as $k_n<k<k_{n+1}$, with $k_n=\lambda^n$ and λ being an arbitrary scale parameter ($\lambda>1$), usually taken equal to 2. In the equations, only quasi-local couplings between nearest and next to nearest neighbor shells are kept.

Recently, a new class of shell models based upon the helical decomposition of NS equations[19] has been suggested[20] and studied.[21] In this way, it is possible to obtain a second non positive defined invariant closer to the NS helicity. The models, which have now two complex variables per shell (u_n^+ and u_n^-, transporting positive and negative helicity, respectively) are simple generalizations of the GOY model. From now on we will concentrate only on one of them (see below), which has been previously shown to share many properties with true turbulent three-dimensional flows.[21]

In particular, in Ref. 21 it has been shown that this model has the *same* degree of intermittency found experimentally in fully developed turbulence, if the set of free parameters is chosen in order to conserve energy and helicity in the inviscid and unforced limit.

Shell models can be thought of as field problems in zero spacial dimension: Their obvious limitation consists in treating all degrees of freedom in a Fourier shell at once; the physical object they describe are coherent planar waves, filling the whole volume of the fluid.

Real turbulence consists of localized eddies of all sizes that interact, merge and subdivide locally: The physical picture is that of a large eddy which decays into smaller eddies. The number of degrees of freedom in such a field problem in d dimensions grows with the wave number as $N(k)\sim k^d$ ($d=0$ in shell models).

The first step in reproducing this kind of hierarchical structure is to transform a *chain* model into a *tree* model with $d=1$. This is achieved by letting grow the number of degrees of freedom with the shell index n as 2^n.

As in the original shell models, this tree model must be in some sense reminiscent of the NS equations. It can be regarded as describing the evolution of the coefficients of an orthonormal wavelets expansion of a one-dimensional projection of the velocity field $v(x,t)$:

$$v(x,t)=\sum_{n,j} \hat{v}_{n,j}(t)\,\psi_{n,j}(x). \tag{5}$$

Here $\psi_{n,j}(x)$ are a complete orthonormal set of wavelets generated from an analyzing wavelet $\psi_{0,0}(x)$ by discrete translations and dilations:

$$\psi_{n,j}(x)=2^{n/2}\psi_{0,0}(2^n x-j). \tag{6}$$

In principle, it is possible to plug the three-dimensional generalization of (6) in the NS equations and deriving an exact

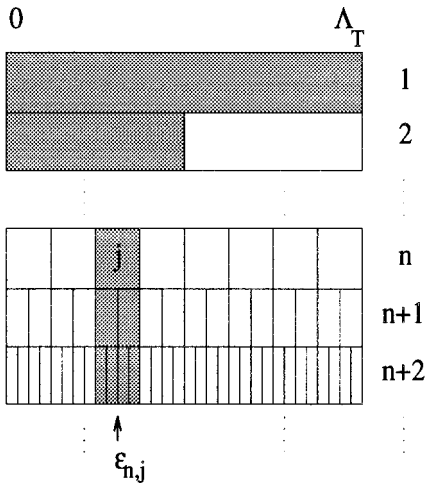

FIG. 1. A picture of the hierarchical system, covering the one-dimensional interval $[0,\Lambda_T]$.

dynamical evolution for the wavelet coefficients.[22] For the sake of simplicity, we will be interested in approximated one-dimensional truncation of the wavelet resolved dynamics. In particular, we can construct dynamical equations of the type of shell models for our tree variables, viewed as the analogues of the expansion coefficients $\hat{v}_{n,j}$. Similar wavelet decomposition, but with purely stochastic coefficients $\hat{v}_{n,j}$ have been used for defining synthetic multi-affine signals.[23]

In Fig. 1, we pictorially show our tree structure, covering the one-dimensional interval $[0,\Lambda_T]$. Each dynamical variable $\hat{v}_{n,j}$ is represented by a box of length $l_n=2^{-n}$, occupying the region $\Lambda_j(n)$ ranging from $(j-1)l_n$ to jl_n. At each scale n there are 2^{n-1} boxes, covering a total length $\Lambda_T=2^{n-1}l_n=1/2$.

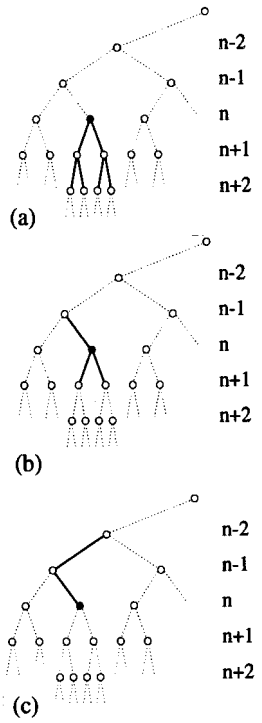

FIG. 2. Pictorial representation of nonlinear interactions of Eq. (9).

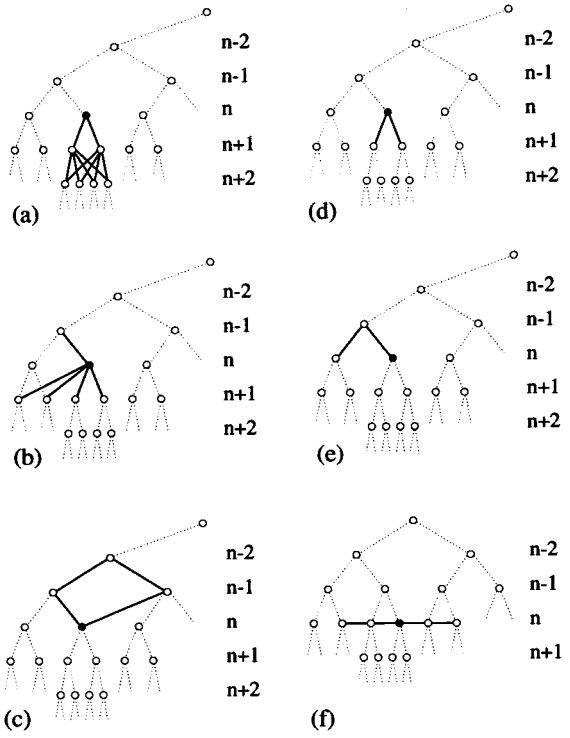

FIG. 3. Pictorial representation of nonlinear interactions of Eq. (11).

For the sake of convenience we define the tree model in terms of *density* variables, $u_{n,j}$ (depicted as balls in Figs. 2 and 3, which would correspond to $\hat{u}_{n,j}=2^{n/2}\hat{v}_{n,j}$ in a wavelet expansion. In this notation, $|u_{n,j}|^2$ represents the energy density in a flow structure of length $l_n=2^{-n}$ and spatially labeled by the index j.

III. THE TREE MODEL

We have chosen the helical shell model studied in Ref. 21 as the starting point for the construction of our hierarchical structure. The dynamical equations of this shell model are the following:

$$\dot{u}_n^+ = ik_n(au_{n+1}^+u_{n+2}^- + bu_{n-1}^+u_{n+1}^- + cu_{n-2}^-u_{n-1}^- +)^* - \nu k_n^2 u_n^+ + \delta_{n,n_0}F^+, \tag{7}$$

and the same holds, with all helicities reversed, for $\dot{u}_n^-$. Here, $n=1,\ldots,N$, where N is the total number of shells, ν is the viscosity, F^+ the external forcing acting on a large-scale shell n_0 and a,b,c are three parameters, which are determined by imposing conservation of energy and helicity in the inviscid and unforced limit:

$$\frac{dE}{dt}=\frac{d}{dt}\left(\sum_n \left(|u_n^+|^2+|u_n^-|^2\right)\right)=0,$$
$$\frac{dH}{dt}=\frac{d}{dt}\left(\sum_n k_n(|u_n^+|^2-|u_n^-|^2)\right)=0. \tag{8}$$

The statistical properties of this model have been studied in Ref. 21: the system turned out to have an intermittent energy transfer very similar to what one can find in the original NS equations.

Hereafter we will fix the intershell separation $\lambda=2$. For this particular (and standard) choice, we must fix $a=1$, $b=-5/12$ and $c=-1/24$.

We introduce a spatial degree of freedom in the system by using the notation $u^{\pm}_{n,j}$ to indicate the complex helical variable on scale n and spatial position labeled by the index j. For a given shell n, the index j can vary from 1 to 2^{n-1}.

In this tree structure, each variable $u_{n,j}$ continues to interact with the nearest and next nearest levels, as in Eq. (7); however, a variety of possibilities is now opened by the presence of many horizontal degrees of freedom localized on each shell. The simplest choice is depicted in Fig. 2, where a portion of the tree structure is shown and the evolving in time variable, $u_{n,j}$, is represented by a black ball. In the figure, solid lines connect interacting balls (variables).

The dynamical tree equations are as follows:

$$\begin{aligned}\dot{u}^{+}_{n,j}=ik_n\{&a/4[u^{+}_{n+1,2j-1}(u^{-}_{n+2,4j-3}+u^{-}_{n+2,4j-2})\\&+u^{+}_{n+1,2j}(u^{-}_{n+2,4j-1}+u^{-}_{n+2,4j})]\\&+b/2[u^{+}_{n-1,\bar{J}}(u^{-}_{n+1,2j-1}+u^{-}_{n+1,2j})]\\&+c[u^{-}_{n-2,\bar{\bar{J}}}u^{-}_{n-1,\bar{J}}]\}^{*}-\nu k_n^2u^{+}_{n,j}+\delta_{n,n_0}F^{+},\end{aligned}\tag{9}$$

where, in the indices, $\bar{\bar{J}}$ is the integer part of $((j+3)/4)$ and $\bar{J}$ is the integer part of $((j+1)/2)$.

The interaction terms with coefficients $a/4$, $b/2$ and c are depicted in Figs. 2(a), 2(b), and 2(c), respectively.

The same equation holds, with all helicities reversed, for $\dot{u}^{-}_{n,j}$. The numerical values of a, b and c are the same as the original helical shell. In the unforced and inviscid limit our system conserves the total energy and helicity, namely,

$$\begin{aligned}\frac{dE}{dt}&=\frac{d}{dt}\left(\sum_{n,j}2^{-n}|u^{+}_{n,j}|^2+|u^{-}_{n,j}|^2\right)=0,\\\frac{dH}{dt}&=\frac{d}{dt}\left(\sum_{n,j}2^{-n}k_n|u^{+}_{n,j}|^2-|u^{-}_{n,j}|^2\right)=0.\end{aligned}\tag{10}$$

Let us be reminded that our tree variables can be roughly viewed as the one-dimensional model counterparts of the amplitudes, $\hat{u}_{nj}=2^{n/2}\hat{v}_{nj}$, in a wavelet expansion of the velocity field [see Eq. (6)].

This analogy must be carried only on qualitative grounds, in particular if one considers that, in the wavelet basis, the Laplacian of the viscous term is not diagonal and that we have drastically reduced the possible interactions among variables. However, in a wavelet expansion, we expect the nonlinear and dissipation terms to be large only if the involved scales are of similar sizes: This corresponds to the physical property that eddies in a fluid mainly transfer energy to eddies of similar scale. Also interaction among the position indices can be expected to be localized, with the precise degree of localization depending on the details of the wavelet basis.

Besides the simple implementation (9), one can build up more complex equations, simply turning on new interactions among variables (always conserving energy and helicity). The guideline in restricting the possible choices can be phenomenologically motivated by requiring a certain degree of locality, both in Fourier and real spaces.

As an example, an enlarged set of interactions is depicted in Fig. 3: in particular two contributes reminiscent of the Desnyansky–Novikov (DN) shell model[24] have been added [see Figs. 3(d) and 3(e)]. Structurally new interactions are those depicted in Fig. 3(f), where only horizontal couplings are considered.

By putting them all together we have

$$\begin{aligned}\dot{u}^{+}_{n,j}=ik_n\{&a/4[(u^{+}_{n+1,2j-1}+u^{+}_{n+1,2j})(u^{-}_{n+2,4j-3}+u^{-}_{n+2,4j-2}+u^{-}_{n+2,4j-1}+u^{-}_{n+2,4j})]+b/2[u^{+}_{n-1,\bar{J}}(u^{-}_{n+1,2j-1}\\&+u^{-}_{n+1,2j}+u^{-}_{n+1,2\tilde{J}-1}+u^{-}_{n+1,2\tilde{J}})]+c[u^{-}_{n-2,\bar{\bar{J}}}(u^{-}_{n-1,2\bar{\bar{J}}-1}+u^{-}_{n-1,2\bar{\bar{J}}})]\\&+d[-u^{-}_{n+1,2j-1}u^{+}_{n+1,2j}-u^{+}_{n+1,2j-1}u^{-}_{n+1,2j}+e_1u^{-}_{n,\tilde{J}}u^{+}_{n-1,\bar{J}}\\&+e_2u^{-}_{n,\tilde{J}}u^{-}_{n-1,\bar{J}}]+f[u^{+}_{n,j+1}u^{-}_{n,j+2}-u^{+}_{n,j-1}u^{-}_{n,j+1}-u^{-}_{n,j-1}u^{+}_{n,j+1}+u^{-}_{n,j-2}u^{+}_{n,j-1}]\}^{*}-\nu k_n^2u^{+}_{n,j}+\delta_{n,n_0}F^{+},\end{aligned}\tag{11}$$

where, in the indices $\bar{\bar{J}}$ is the integer part of $((j+3)/4)$, $\bar{J}$ is the integer part of $((j+1/2))$ and $\tilde{J}$ stays for the index $(j-1)$ if j is even and for the index $(j+1)$ if j is odd.

The interaction terms with coefficients $a/4$, $b/2$, c, d and f are depicted in Figs. 3(a), 3(b), 3(c), 3(d)–(e) and 3(f), respectively. In considering the horizontal interactions of Fig. 3(f), the tree must be viewed as leaving on the surface of a cone, with the last position j on each level connected to the first one on the same level.

All coefficients in the nonlinear terms of (11) are chosen in order to conserve the total energy and helicity (10) of the system. Each of the three interactions types (GOY, DN and horizontal) conserves separately E and H: this leaves some freedom only in the choice of the two relative weights d and f in (11). We fixed $d=f=1$; while the coefficients a,b,c are the same as before and $e_1=3/4$ and $e_2=1/4$.

In our simulations we have considered both the simple version of the hierarchical system described by (9) and by

Fig. 2, which we will call version A, and the more complete description by (11) and by Fig. 3, denoted hereafter as version B.

IV. NUMERICAL RESULTS

A. Numerical implementation

In our simulations we have considered a total number of levels $N=16$. The total number of sites forming the tree is then $N_T=2^N-1=65535$, each one described in terms of two complex variables.

When dealing with this tree structure, the computer effort needed for numerical simulations increases enormously with respect to the original chain model: in order to collect reliable statistics a computing time of $O(10^4)$ longer is now needed.

For this reason, we have implemented our numerical experiments on the APE-100 machine.[25]

APE-100 is a single instruction multiple data (SIMD) parallel architecture, based on a three-dimensional cubic mesh of nodes with periodic boundary conditions, each node being connected to its 6 neighbors. The particular version we used is a 512-node configuration, with a floating point performance of 50 Mflops peak speed on a single processor. Each processing node contains a floating point 32 bit real arithmetics processor and a 4 Mbyte local memory.

We used the parallelism of this machine in the simplest way, its 512 processors integrate simultaneously the same equations, starting from different initial conditions. A good statistics is then obtained by time-averaging on each single processor and ensemble-averaging over all processors.

In both cases A and B, we put the following parameters values into the dynamical equations:

$$\begin{aligned} &N=16,\\ &\nu=2.0\times10^{-5},\\ &F^{\pm}=(5.0\times10^{-3},5.0\times10^{-3}),\\ &n_0=1,\\ &k_0=6.25\times10^{-2}. \end{aligned} \tag{12}$$

We used the Runge–Kutta fourth-order method in integrating the system, with a time step varying from 10^{-3} to 5.0×10^{-4} time units, depending on case A or B. In both cases we integrated the model for a total number of steps of the order of 10^5 on each processor of the parallel machine; considering all processors, we were able to collect a total statistics of 500 eddy-turnover times, using a few days of computing time.

B. Synchronization

Before considering the statistical properties of the system, let us mention a dynamical effect which emerged immediately in numerical integrations, that is, synchronization on the last (dissipative) levels.

Even starting to integrate from an initial configuration having different values on different sites of each tree level, dynamical variables on nearby locations in the last shells (i.e., in the dissipative range) synchronize after relatively few time steps.

The mechanism underlying this phenomenon can be easily understood if one considers what follows: at the viscous cutoff (which corresponds in our case to $n_d\sim11$), the ratio between variables belonging to two successive scales $|u_n|/|u_{n-1}|$ undergoes an abrupt decrease, when passing from the inertial range ($n\leqslant n_d$) to the viscous range ($n>n_d$). Then, in the dynamical equation for $n=n_d$, interactions involving the upper levels become largely predominant with respect to the others: this naturally leads to a similar behavior of variables sitting on two close locations, whose dynamics turns out to be governed by essentially the same equation. This synchronization is then transmitted and spread out into lower levels, in which nearby variables become equal in groups of 4, 8, 16, ..., and so on, as the shell index n increases.

In both cases A and B, this synchronization does not affect the inertial shells. In the version A of the model this process starts already from $n^*=11$. In case B the situation changes: the horizontal interactions are quite effective in breaking the synchronization on two close sites nearby the dissipative cutoff and synchronization effects are thus shifted towards the very last levels ($n=15$ and 16, in our case).

C. The energy dissipation field

The first step in constructing the energy dissipation field of our model is to consider the following function:

$$\eta_{n,j}=\nu k_n^2(|u_{n,j}^+|^2+|u_{n,j}^-|^2), \tag{13}$$

which represents the energy dissipation *density* in the structure covering the region $\Lambda_j(n)$ of length 2^{-n}, centered in the spatial site labeled by j. These structures are represented by boxes in Fig. 1.

The total energy dissipation density, $\epsilon=(1/\Lambda_T)\int_{\Lambda_T}\epsilon(x)dx$, where Λ_T is the total space length, is, by definition, the sum of all these contributions (sum over boxes at all scales in Fig. 1):

$$\epsilon=\sum_{n,j}2^{-n}\eta_{n,j}. \tag{14}$$

On the other hand, in order to study the scaling properties of the energy dissipation field, one has to disentangle in ϵ the contributions coming from the coarse-grained energy dissipation field ϵ_r, as defined in Sec. I, Eq. (2). In our formulation, we can then rewrite as follows:

$$\begin{aligned} \epsilon&=\frac{1}{\Lambda_T}\int_{\Lambda_T}\epsilon(x)dx\\ &=\frac{1}{2^{n-1}}\sum_{j=1}^{2^{n-1}}\left(\frac{1}{2^{-n}}\int_{\Lambda_j(n)}\epsilon(x)dx\right)=\frac{1}{2^{n-1}}\sum_{j=1}^{2^{n-1}}\epsilon_{n,j}, \end{aligned} \tag{15}$$

where the last expression is independent of n and the $\epsilon_{n,j}$'s are the coarse-grained energy dissipation densities, obtained as averages over spatial regions of length 2^{-n}. Note that the

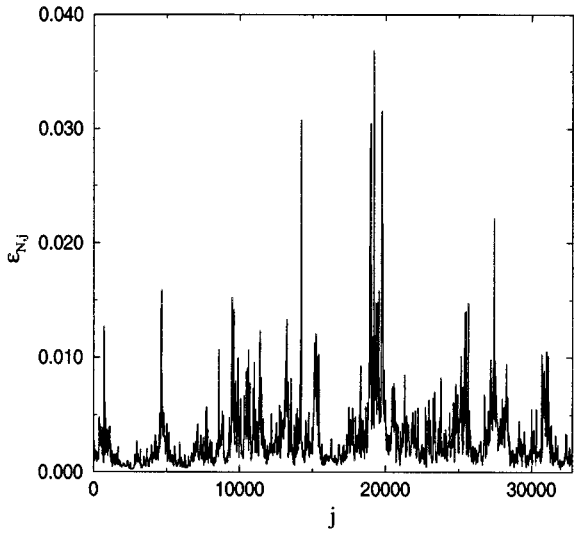

FIG. 4. Instantaneous configuration of the coarse-grained energy dissipation density field, $\epsilon_{N,j}$, over the last level sites (version B).

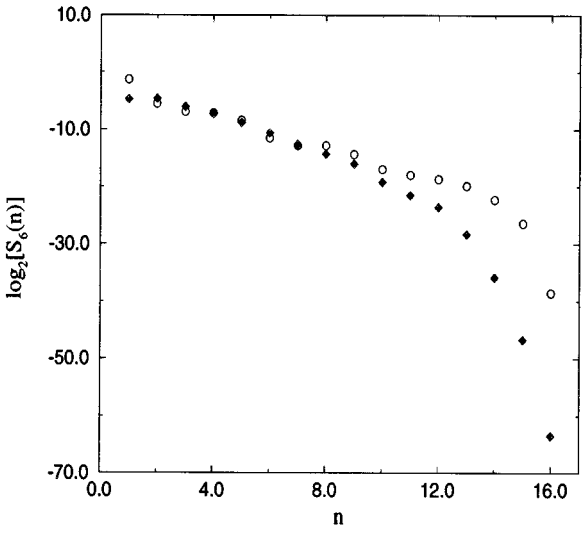

FIG. 5. Log–log plot of the sixth order velocity field structure function, $S_6(n)$, against the wave number k_n, for versions A (white circles) and B (black diamonds).

average density $\epsilon_{n,j}$ over $\Lambda_j(n)$ does not coincide simply with the density $\eta_{n,j}$ of the structure living in $\Lambda_j(n)$, namely,

$$\epsilon_{n,j}=\eta_{n,j}+\sum_{m<n}\eta_{m,k(m)}+\sum_{m>n}\langle\eta_{m,k(m)}\rangle_{I(m)}. \tag{16}$$

Here, in the second (third) term of the rhs we take into account density contributions coming from larger (smaller) scale structures (as an example, all regions contributing to the definition of $\epsilon_{n,j}$ are represented as shadowed boxes in Fig. 1). The index $k(m)$ in the second term of rhs labels the location of larger scale structures containing the region $\Lambda_j(n)$ under consideration (shadowed boxes with $m<n$ in Fig. 1). In the third term, an average is performed over $k(m)\in I(m)$, where $I(m)$ labels the set of structures contained in $\Lambda_j(n)$, for any $m>n$ [in Fig. 1, $I(m)$ labels the two boxes at $n+1$, the four boxes at $n+2$ and so on].

The best spatially resolved energy dissipation field is for $n=N$,

$$\epsilon_{N,j}=\sum_{m\leqslant N}\eta_{m,k(m)};\quad j=1,\ldots,2^{N-1}. \tag{17}$$

In Fig. 4, the instantaneous values assumed by $\epsilon_{N,j}$ in the $N_T/2=32768$ locations of the last level are showed. The chaotic, intermittent character of this spatial signal is evident.

D. Scaling laws and the refined Kolmogorov hypothesis

Performing long-time numerical integrations of Eqs. (9) and (11), we have studied the statistical properties of both versions A and B of our tree model. We have investigated the scaling properties of velocity field structure functions, $S_p(n)$, and of coarse-grained energy dissipation moments, $D_p(n)$.

These moments have been evaluated by time, space and ensemble-averaging our variables over the total integration time, the spatial locations and the processors of the APE machine:

$$\begin{aligned}S_p(n)&\equiv\sum_{m,t,j}\frac{1}{MT2^n}(\sqrt{|u^+_{n,j}(t,m)|^2+|u^-_{n,j}(t,m)|^2})^p,\\ D_p(n)&\equiv\sum_{m,t,j}\frac{1}{MT2^n}\epsilon^p_{n,j}(t,m),\end{aligned} \tag{18}$$

where m is the processor index (varying from 1 to $M=512$) and t is the time step index.

These moments are expected to follow, in the inertial range, the scaling laws [see Eqs. (1), (2)]:

$$\begin{aligned}S_p(n)&=k_n^{-\zeta(p)},\\ D_p(n)&=k_n^{-\tau(p)},\end{aligned} \tag{19}$$

with the two scaling exponents related together by the RKH relation (4), eventually.

In Fig. 5, the log–log plot of the sixth order structure function $S_6(n)$ against k_n is presented for the two versions A and B: the two different slopes in the inertial range indicate a degree of intermittency strongly dependent on how the variables of the tree interact.

Let us notice that in both versions A and B, the interaction range in Fourier space is the same (a typical eddy at scale n interacts always with the nearest and next nearest scales $n-1$, $n+1$, $n-2$ and $n+2$); nevertheless, in the two cases the interaction range in physical space is different and a different number of connections between scales is considered. This seems to be of primary importance in determining the intermittency degree of the system.

In order to obtain a quantitative measure of the structure functions scaling exponents, we performed a fit over the inertial range shells, using extended self similarity (ESS):[2] in Fig. 6, the logarithm of the sixth order moment $S_6(n)$ against

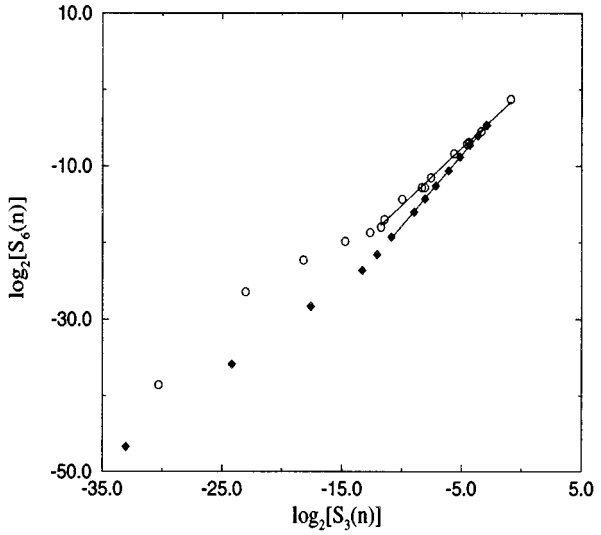

FIG. 6. Log–log plot of the sixth order velocity field structure function, $S_6(n)$, against the third order velocity field structure function, $S_3(n)$, for versions A (white circles) and B (black diamonds). Straight lines correspond to a linear fit in the inertial range. The corresponding slopes are reported in Table I.

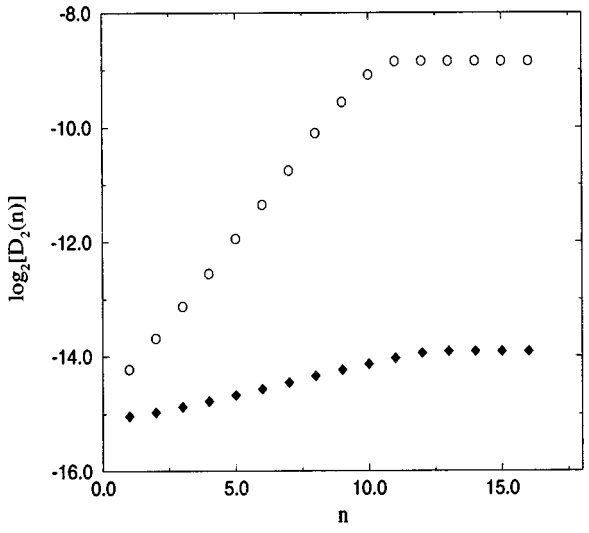

FIG. 7. Log–log plot of the second moment, $D_2(n)$, of energy dissipation density against the wave number k_n, for versions A (white circles) and B (black diamonds).

the logarithm of the third order moment $S_3(n)$ is plotted, again for both versions A and B. The resulting exponents, $\zeta(p)/\zeta(3)$, obtained for all the moments $p=1,\ldots,8$, are reported in Table I and compared with the K41 nonintermittent prediction $p/3$.

We found a similar scaling behavior for the energy dissipation moments: as an example, we show in Fig. 7 the log–log plot of $D_2(n)$ against k_n; again, the reduced steepness in case B indicates a less intermittent behavior, with $\tau(p)$ closer to the zero value.

The subsequent step was to test the RKH for our tree model: to improve the fitting procedure, we applied the ESS method to the RKH relation:[2]

$$S_p(n)=(S_3(n))^{p/3}D_{p/3}(n). \tag{20}$$

Plotting the lhs of this equation against the rhs in a log–log plot, one can directly test the validity of relation (4) in the inertial region: in Fig. 8 three cases, with $p=4$, 5, 6, are reported, for the version A; the same, but for version B, are in Fig. 9. In both versions A and B and for all the moments considered, our fits confirm that the RKH is well satisfied, being all the slopes in the inertial region equal to 1 within a few percent.

The tree-like structure imposed on the velocity fluctuations does not necessarily imply that the energy dissipation can be described in terms of fragmentation processes. In order to test the scale-organization of the energy structures, ultrametric-sensitive observables should be studied.

TABLE I. The scaling exponents ratios, $\zeta(p)/\zeta(3)$ $(p=1,\ldots,8)$, resulting from the ESS fitting procedure. The values obtained for versions A and B are reported in the second and third column, respectively. In the last column there are the K41 values.

p	A	B	$K41$
1	0.41 ± 0.01	0.348 ± 0.005	0.333
2	0.74 ± 0.01	0.682 ± 0.005	0.667
3	1	1	1
4	1.21 ± 0.01	1.303 ± 0.006	1.333
5	1.36 ± 0.02	1.59 ± 0.01	1.667
6	1.48 ± 0.03	1.86 ± 0.02	2
7	1.55 ± 0.05	2.12 ± 0.03	2.333
8	1.60 ± 0.07	2.35 ± 0.03	2.667

V. CONCLUSIONS

A new class of dynamical models in one spatial dimension which shows spatial and temporal chaos (fully developed turbulence) has been introduced and numerically studied. The model originates from a wavelet-like decomposition

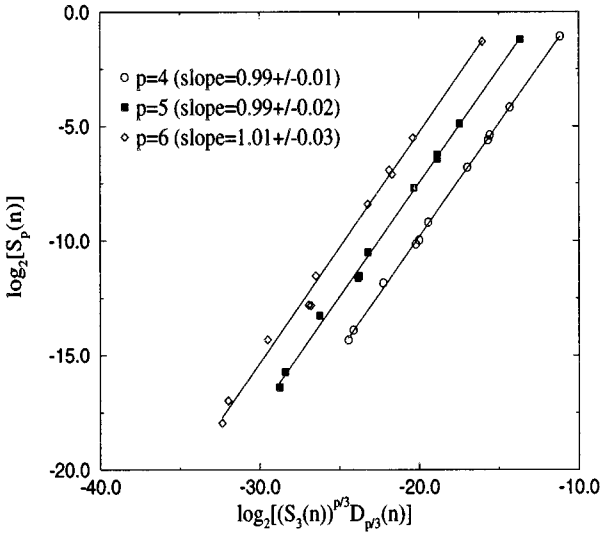

FIG. 8. Log–log plot of the velocity field structure functions, $S_p(n)$ $(p=4,5,6)$, against $((S_3(n))^{p/3}D_{p/3}(n))$ in the inertial range, for version A. Straight lines correspond to a linear fit: all cases are compatible with the RKH.

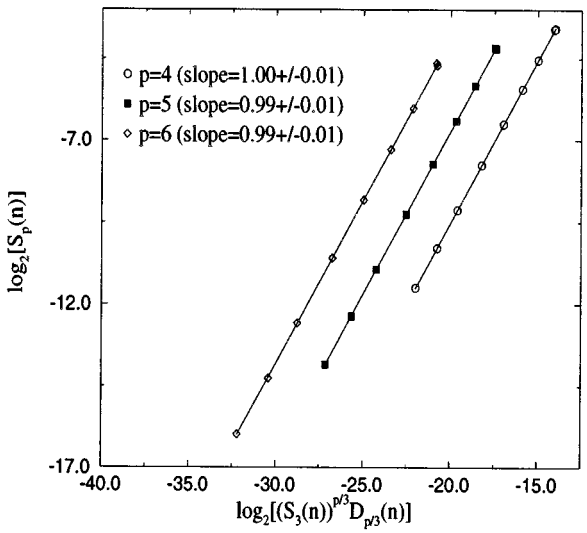

FIG. 9. The same as in Fig. 8, but for version B.

of a one-dimensional cut of a turbulent velocity field. Mainly local interactions in space and in scale are retained.

Structure function scaling, as well as spatial fluctuations of the energy dissipation, show the typical multifractal behavior of a real turbulent flow. Refined Kolmogorov hypothesis linking the statistics of structure functions to the coarse-grained energy dissipation is found to hold within a few per cent. These kinds of models open the possibility of investigating numerically many open questions of turbulence. Among them, work is in progress for detecting possible ultrametric structure in the energy cascade mechanism.[26]

The presence of real space allows us also to test in a quantitative way some of the most popular eddy-viscosity models used for simulating small-scale activity in large-eddy-simulations.

Our results show that intermittency strongly depends on the degree of tree connectiveness. For example, by passing from version A to version B one observes a decrease in the deviations $\delta\zeta(p)=|\zeta(p)-p/3|$ from Kolmogorov scaling (from $\sim$30% in case A to $\sim$10% in case B): This is probably due to the presence of horizontal couplings in version B which allow a better efficiency in the energy exchanges. Increasing the number of triad-couplings should enlarge the number of possible downward paths followed by the energy cascade.

This tendency toward a less intermittent regime, by increasing the number of triad interactions, may seem in contrast with the observed intermittency in the original Navier–Stokes equations (which have all possible interactions switched on). This contradiction is only apparent: Divergenceless character of the original NS field, added to complicated phase-coherence effects, can very easily introduce different dynamical weights in the possible triad interactions leading to a situation where only a few of them govern the global dynamical evolution. For example, Grossmann and coworkers showed, by performing suitable truncation of NS equations, that intermittency depends on the typical degree of locality in Fourier space of the survived triad interactions; very similar results have also been found in shell models at varying the inter-shell ratio λ;[27] the question of finding universal observables in hydrodynamics-like intermittent systems remains of primary interest.[27–29]

ACKNOWLEDGMENTS

Interesting discussions with E. Aurell and D. Lohse are kindly acknowledged. During the preparation of this paper we have received a preprint by E. Aurell, E. Dormy and P. Frick on a similar generalization of shell models for two-dimensional turbulence. They give a slightly different explanation for synchronization of small scale dynamics.

[1] A. N. Kolmogorov, ''The local structure of turbulence in incompressible viscous fluid for very large Reynolds numbers,'' Dokl. Akad. Nauk SSSR **30**, 9 (1941).
[2] R. Benzi, S. Ciliberto, R. Tripiccione, C. Baudet, C. Massaioli, and S. Succi, ''Extended self–similarity in turbulent flows,'' Phys. Rev. E **48**, R29 (1993); R. Benzi, S. Ciliberto, C. Baudet, and G. R. Chavarria, ''On the scaling of three–dimensional homogeneous and isotropic turbulence,'' Physica D **80**, 385 (1994).
[3] C. Meneveau and K. R. Sreenivasan, ''Simple multifractal cascade model for fully developed turbulence,'' Phys. Rev. Lett. **59**, 1424 (1987).
[4] A. N. Kolmogorov, ''A refinement of previous hypotheses concerning the local structure of turbulence in a viscous incompressible fluid at high Reynolds number,'' J. Fluid Mech. **13**, 82 (1962).
[5] G. Stolovitzky and K. R. Sreenivasan, ''Kolmogorov's refined similarity hypothesis for turbulence and general stochastic processes'', Rev. Mod. Phys. **66**, 229 (1994).
[6] R. Benzi, G. Paladin, G. Parisi, and A. Vulpiani, ''On the multifractal nature of fully developed turbulence and chaotic systems,'' J. Phys. A **17**, 3521 (1984).
[7] Z. S. She and E. Leveque, ''Universal scaling laws in fully developed turbulence,'' Phys. Rev. Lett. **72**, 336 (1994).
[8] A. M. Oboukhov, ''On the problem of nonlinear interactions in fluid dynamics,'' Gerlands Beitr. Geophys., Leipzig **82**, 282 (1973).
[9] A. B. Glukhovsky, ''Stability of nonlinear chain-type systems used to model cascaded energy transfer processes,'' Atmos. Ocean. Phys. **11**, 491 (1975).
[10] J. Eggers and S. Grossmann, ''Anomalous turbulent velocity scaling from the Navier–Stokes equation,'' Phys. Lett. A **156**, 444 (1991); ''Does deterministic chaos imply intermittency in fully developed turbulence?,'' Phys. Fluids A **3**, 1958 (1991).
[11] S. Grossmann and D. Lohse, ''Intermittency in the Navier–Stokes dynamics,'' Z. Phys. B **89**, 11 (1992); ''Intermittency in turbulence,'' Physica A **194**, 519 (1993); ''Scale resolved intermittency in turbulence,'' Phys. Fluids **6**, 611 (1994).
[12] L. Kadanoff, ''A model of turbulence,'' Phys. Today **48**, 11 (1995).
[13] E. B. Gledzer, ''System of hydrodymamic type admitting two quadratic integrals of motion,'' Sov. Phys. Dokl. **18**, 216 (1973).
[14] M. Yamada and K. Ohkitani, ''Lyapunov spectrum of a chaotic model of three–dimensional turbulence,'' J. Phys. Soc. Jpn. **56**, 4210 (1987); ''Temporal intermittency in the energy cascade process and local Lyapunov analysis in fully developed turbulence,'' Prog. Theor. Phys. **81**, 329 (1989).
[15] M. H. Jensen, G. Paladin, and A. Vulpiani, ''Intermittency in a cascade model for three dimensional turbulence,'' Phys. Rev. A **43**, 798 (1991).
[16] L. Biferale, A. Lambert, R. Lima, and G. Paladin; ''Transition to chaos in a shell model of turbulence,'' Physica D **80**, 105 (1995).
[17] D. Pisarenko, L. Biferale, D. Courvoisier, U. Frisch, and M. Vergassola, ''Further results on multifractality in shell models,'' Phys. Fluids A **65**, 2533 (1993).
[18] L. Kadanoff, D. Lohse, J. Wang, and R. Benzi, ''Scaling and dissipation in the GOY shell model,'' Phys. Fluids **7**, 617 (1995).
[19] F. Waleffe, ''The nature of triad interactions in homogeneous turbulence,'' Phys. Fluids A **4**, 350 (1992).
[20] L. Biferale and R. Kerr, ''Role of inviscid invariants in shell models of turbulence,'' Phys. Rev. E **52**, 6113 (1996).
[21] R. Benzi, L. Biferale, R. Kerr, and E. Trovatore, ''Helical shell models for three dimensional turbulence,'' Phys. Rev. E **53**, 3541 (1996).
[22] T. Nakano, ''Direct Interaction approximation of turbulence in the wave packet representation,'' Phys. Fluids **31**, 1420 (1988).

[23]R. Benzi, L. Biferale, A. Crisanti, G. Paladin, M. Vergassola, and A. Vulpiani, ''A random process for the construction of multiaffine fields,'' Physica D **65**, 352 (1993).
[24]V. N. Desnyansky and E. A. Novikov, ''Evolution of turbulence spectra to self–similar regime,'' Izv. Akad. Nauk SSSR Fiz. Atmos. Okeana **10**, 127 (1974).
[25]C. Battista and the APE Collaboration, ''The APE–100 computer: the architecture,'' Int. J. High Speed Comput. **5**, 637 (1993).
[26]J. O'Neil and C. Meneveau, ''Spatial correlations in turbulence: Predictions from multifractal formalism and comparison with experiments,'' Phys. Fluids A **5**, 158 (1993).
[27]R. Benzi, L. Biferale, and E. Trovatore, ''Universal statistics of non-linear energy transfer in turbulent models,'' Phys. Rev. Lett. **77**, 3114 (1996).
[28]Z. S. She and E. C. Waymire, ''Quantized energy cascade and log–Poisson statistics in fully developed turbulence,'' Phys. Rev. Lett. **74**, 262 (1995).
[29]S. Grossmann, D. Lohse, and A. Reeh, ''Developed turbulence: From full simulations to full mode reductions,'' preprint (1996).